A Horizontal Thermal Gradient Cloud Condensation Nucleus Spectrometer[1]

N. FUKUTA AND V. K. SAXENA[2]

Department of Meteorology, University of Utah, Salt Lake City 84112

(Manuscript received 23 January 1979, in final form 21 June 1979)

ABSTRACT

A new cloud condensation nuclei (CCN) spectrometer capable of simulating the desired range of cloud supersaturation in a single chamber is developed. It can rapidly and continuously measure and display the spatial and temporal distributions of the CCN activity spectrum with high resolution and is suitable for airborne, field and laboratory studies. Details of the spectrometer design for producing a range of supersaturations in the sample air flow, controlled size of activated droplets for detection, and of mechanisms for continuous sampling, scanning and recording are presented. The dependency of the plateau in number concentration of the activated CCN on the sample air flow rate and the detection limit are analyzed. The droplet counting mechanism is compared with the direct photographic method and is found in reasonable agreement. The usefulness of the spectrometer is demonstrated by detecting the simulated smoke plume in the laboratory in real time. Measurements on an urban aerosol indicate a strong scavenging effect of rain and drizzle on CCN concentrations and a marked diurnal characteristic change in the slope of the CCN activation spectrum.

1. Introduction

An understanding of the cloud microstructure requires a knowledge of the activation spectrum of cloud condensation nuclei (CCN) existing in the cloud-forming air. A new concept of a CCN spectrometer capable of measuring the CCN activity spectrum over a wide range of cloud supersaturations with high resolution in time or space and displaying the results in real time is developed. In the main chamber of the spectrometer, a scheme of producing a range of supersaturations along the median plane by means of a steady-state temperature gradient across the chamber height as well as the breadth of the top and bottom plates is used. The sample air is continually taken into the chamber and pre-processed in order to avoid undesirable transient supersaturation development. It is then allowed to undergo a range of supersaturations for activation. The growth time of droplets after activation is adjusted such that all the activated droplets acquire the same predetermined size at the exit. A sampling probe continuously scans through the range of supersaturations along the median plane and sends the droplets to an optical device for counting them individually. The count and the supersaturation, the latter being identified by the output of a potentiometer coupled with the probe position by means of a rack and pinion mechanism, are simultaneously displayed on both coordinates of an X-Y recorder—a form of CCN activity spectrum presentation. The scanning of the range of supersaturations is programmed to repeat after a preset time interval.

The principle of the new spectrometer has been discussed by Fukuta and Saxena (1977). An instrument based on this principle—generally referred to as the CCN spectrometer—has already been fabricated and tested in the laboratory and field. It has also been compared with a conventional CCN counter. It has a capability of producing measurements of the spatial distributions of the CCN spectrum with high resolutions, displaying them in real time. This feature renders it especially useful for airborne measurements. Jiusto (1976) and Radke and Jiusto (1977) have discussed the CCN spectrometer in their recent reviews of CCN counters. In this paper, the design of the CCN spectrometer is elaborated. An attempt is made to describe all relevant design and operational parameters. The test results of the spectrometer by measuring the CCN spectrum of an urban aerosol sample and detecting a smoke plume simulated in the laboratory are discussed.

2. Apparatus

The main section of the CCN spectrometer consists of two copper plates, each 0.64 cm thick, 22.9 cm wide (OD), and 83.8 cm long (for details of dimensions, see Table 1). These plates are placed parallel to each other separated by two side walls, each 1.8 cm

[1] Parts of this paper were presented at the Second International Conference on Cloud Physics, Boulder, CO, 26-30 July 1976.

[2] Present affiliation: Department of Geophysics, North Carolina State University, Raleigh 27650.

0021-8952/79/101352-11$06.75

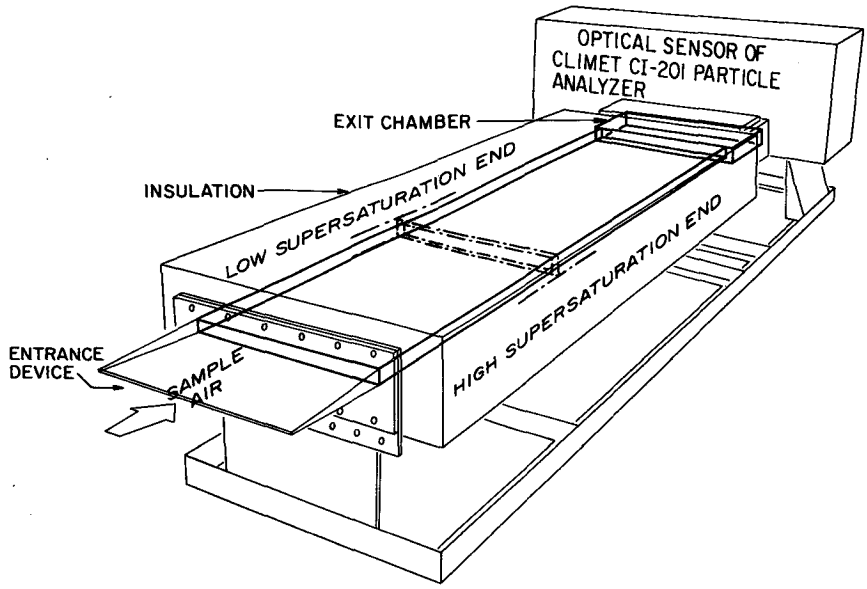

FIG. 1. Perspective view of the aerosol sampling section of the CCN spectrometer.

high. One wall is made of metal, such as brass or stainless steel, while the other is made of a non-conducting material, such as phenolic resin. The material of the metallic wall is dictated by the range of desired supersaturations. The desired range of temperature differences is created by heating the entire edge of the top plate just above the phenolic resin wall and cooling the corresponding edge of the bottom plate. Along the top plate edge of the non-conducting wall side is stretched a nichrome wire electrically insulated from the metal surface. The heating is adjusted by controlling electric current through the wire and the desired temperature is maintained by means of a proportional temperature controller. Along the corresponding edge of the bottom plate is a soldered copper tube through which thermostated water is circulated. Such an arrangement provides flexibility in selecting and operating the desired supersaturation range. The first 16.8 cm length of the bottom plate is kept uncovered and the next 66 cm is entirely covered by a filter paper which is kept saturated with water. This helps establish the steady-state temperature profile before water vapor starts diffusing into the sample and avoids undesirable transient supersaturations (Saxena *et al.*, 1970; Fitzgerald, 1970; Saxena and Fowler, 1973; Naruse, 1978).

A similar arrangement exists at the lower surface of the top plate except along the last 66 cm length. The lengths of the filter paper at different operating supersaturations in the 66 cm length section are adjusted so as to allow longer time for vapor diffusion at smaller supersaturations and vice versa so that at the end of the filter paper, all the activated droplets may attain about the same size. These filter papers are kept wetted by spraying water on their surfaces at regular time intervals. The profile of the filter paper is obtained by trial and error based on the estimates of the growth times and fallout effect. The last 1 cm of the top and bottom plates is left uncovered and painted black for photographing the droplets and withdrawing the sample by inserting a tube ~1 cm deep into the chamber from the exit end. The absence of the filter paper minimizes water condensation on the surface of the sampling tube; however, use of a glass sampling tube lined with plaster of paris, which is automatically kept saturated with

TABLE 1. Specifications of the CCN spectrometer.

1. Chamber dimensions: 83.8 cm (length)×1.8 cm (height) ×19.1 cm (width)(all ID)
2. Supersaturation range: e.g., 0.15–1.2% [variable depending upon the applied temperature difference (see Fig. 2)]
3. Maximum temperature difference for sustaining the above range: 6°C
4. Median plane temperature: slightly higher (1–4°C) than ambient
5. Chamber weight: 26 kg
6. Plate material: copper, 0.64 cm thick
7. Side walls: 1.8 cm (height)×1.9 cm (thickness); one made of brass and the other of phenolic resin
8. Plate area: 1600 cm² (each plate); 1261 cm² (bottom plate covered with the filter paper); 961 cm² (top plate covered with filter paper)
9. Total longitudinal heat transfer* (i.e., along the breadth of metal plates): 32 W
10. Total vertical heat transfer*: 0.64 W (sensible)+2.02 W (latent)+1.77 W (radiative)
11. Time required for the supersaturation to rise from $S=0$ to $S=0.9\,S_m$: ~3.2 s
12. Diameter of the sampling tube (ID): 0.28 cm

* These calculations are done for maximum temperature difference of 6°C across the non-conducting wall.

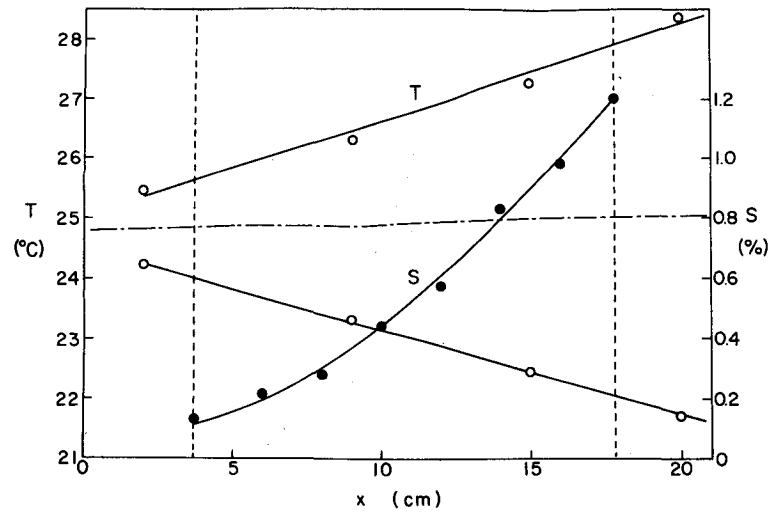

FIG. 2. Plot of the temperature (T) profile across the width (x) of the top and bottom of the main chamber. Vertical dashed lines mark the end positions of the scanning tube which draws sample at different supersaturations (S) along the median plane as indicated by the S profile. The origin of the x axis is at the outer end of the conducting wall.

water due to condensation, completely eliminates the problem. The heating of the entire edge of the top copper plate along the phenolic wall and the cooling of the corresponding edge of the bottom plate, result in a temperature gradient across the breadth of the plates. The whole chamber is kept thermally insulated from the ambient. Fig. 1 shows the perspective view of the spectrometer.

3. Supersaturation field

From the above discussion it is evident that the CCN spectrometer differs from the previously designed dynamic chambers (Storozhilova, 1961; Severynse, 1964; Laktionov, 1967, 1968; Hudson and Squires, 1973; Sinnarwalla and Alofs, 1973) inasmuch as a range of desired supersaturations is maintained rather than only one supersaturation. The supersaturation varies horizontally in a direction at right angles to the sample flow, being maximum near the nonconducting wall and minimum near the conducting wall. If the supersaturation definition of the sample is to be precisely maintained, the following three conditions should be satisfied. First, the temperature profile along the breadth of the chamber plates should be close to linear under the steady state. Second, the sample air flow should be laminar at least after the onset of water vapor diffusion into it. Third, the supersaturation decrement due to wall effects should be sufficiently small.

The first condition was experimentally confirmed to hold within 0.1°C in the present design of the chamber (see Fig. 2). Under the linear horizontal temperature profile along the breadth of the chamber plates, Fukuta and Saxena (1977) showed that the maximum error in the estimation of the operating supersaturation in the range of 0.15–2% based on the assumption of linear vertical profile of temperature and water vapor pressure, is less than 2% of the supersaturation. The supersaturation in our chamber, therefore, can be estimated based on linear vertical fields of temperature and vapor pressure. With the help of a carefully designed sample air introducing device which will be discussed in the following section, establishing Poiseuille flow in the chamber was confirmed through smoke tracer experiments (see Fig. 3). For our present chamber design and a maximum temperature difference of 6°C, the laminar flow forms whenever the flow speed is greater than 1.5 cm s^{-1}. Typically a flow speed of 3 cm s^{-1} is used in the chamber.

For a static chamber of cylindrical symmetry (Twomey, 1963), the supersaturation reducing effect on the wall has been discussed by Elliott (1971). In his estimation, however, he assumed an isothermal wall with a temperature equal to that of the top plate, which apparently induced large decrements of supersaturation as well as wide affected zones. However, the perturbation introduced in the supersaturation field due to wall effects can be practically dispensed with if good thermally conductive walls are used (Gagin and Terliuc, 1968). In such a chamber, a linear vertical temperature profile is maintained on the walls. If the conducting walls are kept dry, the wall effects are eliminated entirely (Goroch and Carstens, 1972). One of the walls in our CCN spectrometer is made of conductive material, although condensation takes place on it under usual operating conditions and it becomes wet. Our recent estimation (Tomlinson and Fukuta, 1979) assuming a wettable

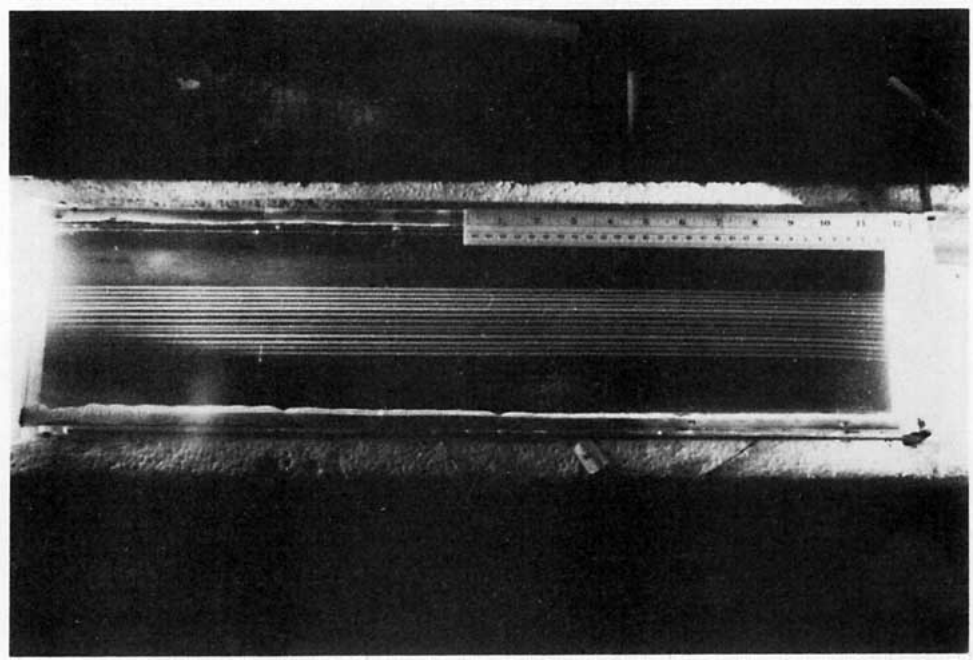

FIG. 3. Smoke test of the air flow in the prototype chamber. Sample air flows from right to left. The upper and lower scales of the ruler are respectively in inches and centimeters. The lower side of the chamber maintains a temperature gradient of 0.23°C cm^{-1} and the average sample air speed is 3.1 cm s^{-1}. The slight bending of smoke on the right-hand side is due to tilting of the smoke introducing pipe.

wall with a linear vertical temperature profile showed that 10% deviation from the supersaturation values estimated under linear vertical profiles of both temperature and vapor pressure occurs within 1 cm from the wall in a chamber of cylindrical shape with the aspect ratio of 10. Our estimation for a rectangular chamber under the same wall conditions (Tomlinson and Fukuta, in press) gives the deviation to occur within 1.5 cm from the wall. If one avoids sampling from the zones within a distance of 1.5 cm from the side walls, the operating supersaturation should fall within 10% of the estimated value. In our chamber, a distance of at least 2 cm adjacent to each wall is left unscanned in order to avoid sampling from the affected zones.

4. Design and fabrication

a. Entrance device and exit chamber

The sample air is drawn through an entrance device from the main sample airstream to the central processing chamber. It consists of a wedge-shaped metal box whose top and bottom plates subtend a 10° angle

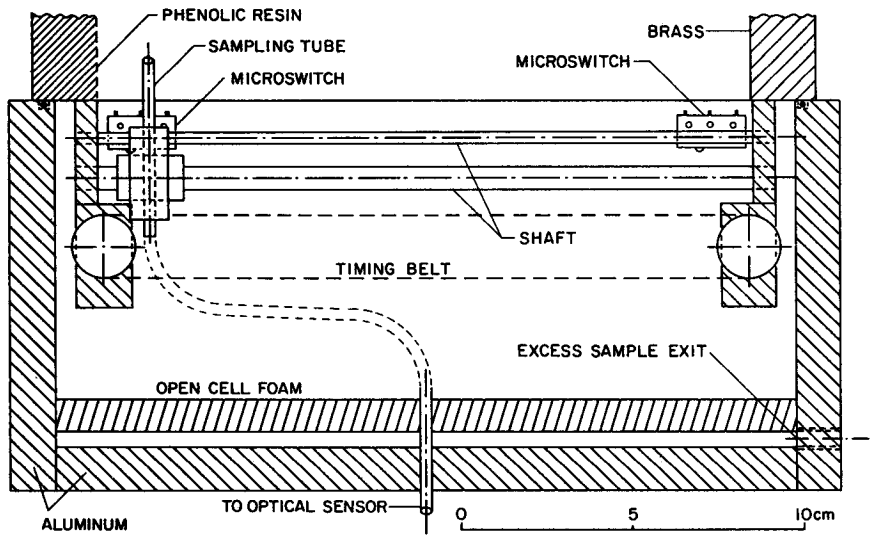

FIG. 4. Top view of the exit chamber with the scanning mechanism of sampling tube.

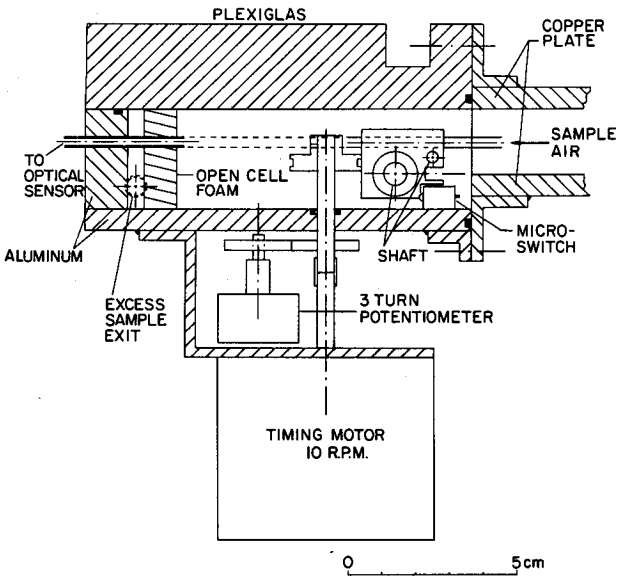

FIG. 5. Side view of the exit chamber and the scanning mechanism of sampling tube.

at the inlet manifold tube that is situated along the median plane of the chamber and at right angles to the sample-flow direction. The two ends of this inlet tube are connected to the sample source through a Y-joint and the sample air flows into the main chamber through a narrow slit whose width is 0.3 mm. Our flow tracer experiments have demonstrated that with such arrangement, the incoming sample smoothly diverges and fills the entire chamber volume under the influence of the applied pressure difference across the inlet tube. Any turbulence existing at the sample entrance subsides shortly thereafter since the viscous forces take over and produce the Poiseuille flow before the water vapor starts diffusing into the sample (see Fig. 3).

To the downstream end of the main chamber is attached a small exit chamber. The purpose of placing an exit chamber is twofold. First, it sustains the laminar flow of the sample air until it is absorbed into a porous wall, and second, it allows detection of activated CCN by moving a sampling tube along the median plane of the main chamber without disturbing the flow. Figs. 4 and 5 show the top and the side views of the exit chamber.

b. Sampling arrangement

A scanning device which holds the sampling tube is placed in the sample air flow passing through the exit chamber. The sampling tube is connected to the optical sensor of the Climet Model CI-201 Particle Analyzer by means of a rubber tube (ID of 0.28 cm and 8.0 cm in length). The scanning device moves on two shafts and is driven by a timing motor at a rate of 10 rpm. The timing motor simultaneously drives a three-turn potentiometer, thereby making a one-to-one correspondence between the sensor position or supersaturation and the voltage output. The voltage of the potentiometer and the number concentration of the activated CCN measured by a pulse-rate technique (voltage), namely, the Climet 201 Particle Analyzer, are fed respectively into the X and Y axes of an automatic fed X-Y chart recorder.[3] The direction of timing motor rotation is reversed every time the scanning device hits one of the two limiting microswitches. When the microswitch at the low supersaturation end is activated, it simultaneously closes the electric circuit of the chart driving mechanism and shifts the chart by a predetermined length. Thus, in 15 s, the sampling tube traverses the entire range of operating supersaturations along the median plane of the chamber. Since the relationships between the voltage of the potentiometer and the supersaturation in the chamber, and the voltage output of the optical sensor and the counts per second are precalibrated, the recorder produces a form of the CCN activation spectrum, the chart being advanced a fixed distance at the end of each spectrum record. This programmed shift on the recorder chart helps obtain legible and comprehensive temporal and spatial distributions of the CCN spectrum on the basis of which real-time decisions could be made during the course of field measurements.

The scanning mechanism shown in Figs. 4 and 5 is suitable for airborne operations. However, because of the length and bending of the rubber tubing, there is a slight possibility of losing activated CCN or droplets. The device shown in Fig. 6 is better in this regard, although it is susceptible to horizontal forces that appear during takeoff, landing and turning of aircraft. The basic difference between the scanning mechanism shown in Fig. 6 and in Figs. 4 and 5 is that in the former, the total weight (~9 kg) of the optical sensor moves back and forth, while in the latter only the sampling tube moves. The sensor box in Fig. 6 is supported by two shafts and the rack and pinion mechanism drives the potentiometer. Instead of reversing the direction of rotation using a single timing motor, two timing motors of different speeds are used with clutches, and they rotate in one direction only. The clutches are activated according to the position of the scanning mechanism by means of a solenoid. The straight sampling tube of the optical sensor scans in a manner similar to that described in Figs. 4 and 5, but in a different exit chamber. This exit chamber consists of a box with one open end passing the activated CCN through and the other holding a lip mechanism. The latter consists of a sheet of open-cell foam rubber placed in front of another closed-cell foam rubber with some air gap between them to apply suction. The sample air is absorbed

[3] Automatic Feed BW-132 X-Y Chart Recorder, Rikadenki Kogyo Co. Ltd., distributed by Soltec Corporation, Encino, CA.

into the first sheet without passing through the second, and is thus continuously removed. While this continues, the sampling tube traverses through a slit which is cut in both the foam rubber sheets along the median plane of the chamber and receives a part of the sample before reaching the absorbing wall. For operations in pressurized aircraft, this lip mechanism does not provide an adequate seal.

The Climet Model CI-201 Particle Analyzer used here has the sensor detached from the electronic circuitry. The sensor is housed in a box which is 51 cm wide, 20 cm high and 19 cm deep. The sensor uses an ellipsoidal mirror and high-intensity filament lamp to detect particles drawn into its chamber. The sample is drawn through a 3.2 mm ID tubing. The light transmitted from one of its focal points is reflected to its second focal point. In the droplet detecting assemply, the view volume of the sample air is situated at the first focal point of the mirror, and the photomultiplier tube is located at the second focal point. Particles drawn into the sensor chamber pass through the view volume, where they are exposed to the high-intensity light beam, causing light to be scattered. Scattered light in the near-forward direction is received at the second focal point and converted into electrical pulses by the photomultiplier tube. Light passing through the view volume is effectively absorbed by the non-reflective cone. The electrical pulses from the photomultiplier tube are amplified by a factor of 10 by the sensor preamplifier circuit.

The sample air stream is drawn into the sensor chamber by a high-speed air pump. Purge air, filtered free of particles >0.1 μm, is drawn, into the sensor chamber through inlets located at the top and the bottom of the sensor chamber. The purge airstream, which contributes to the high performance of the particle analyzer, surrounds the air sample and prevents the sample from diverging as it passes through the sensor chamber. Introduction of the purge airstream into the chamber sweeps residual particles out of the chamber, insuring rapid response to changes in particle concentration and eliminating the necessity for frequent cleaning of the optical components. The purge air and sampled air pass through the pump. The rate of air flow is controlled by a bypass valve, which shunts sensor view volume. The air flow is then applied to a 0.1 μm filter. A portion of the filtered air is returned to the sensor chamber for use as purge air, and the remainder is exhausted through the outlet. The rate of air flow is measured by a flow meter.

The dilution system is employed to slow down the rate at which the sample is introduced into the sensor. This allows conservation of the quantity of the sample needed at each supersaturation. The clean air outlet from the CI-201 Particle Analyzer is fed back into the inlet of the dilution system through a plug-on inlet nozzle assembly. The inlet nozzle assembly consists of concentric nozzles. The outside nozzles takes the outlet air from the particle analyzer and allows it to return to the system. The inner nozzle is utilized as the sampling inlet.

In a leak-proof system, all of the output air of the instrument may be returned to the input and there is no net input. If a small, measured leak on the output line is opened, there will be an equal leak at any opening in the inlet line. The precise outlet leak is measured at the front of the diluter box, while the inlet leak is fed into the center of the sensor flow with an attached fitting. When the system is under operation, 1.2 cm^3 s^{-1} of sample flow escapes through the flow meter and 1.2 cm^3 s^{-1} into the inlet fitting. The sample flow then emerges into the center of the main flow. The particles are accelerated to the velocity of the main stream. Because of the clean air flow of the CI-201 sensor, the particles will remain in the center lamina of the flow and pass through the center of the sensor view volume. Actual mixing of the sample flow does not occur until the flow has entered the exit nozzle. Thus, the inherent problems which occur with mixing-type dilution methods are eliminated in our system. Through this technique, a dilution of one hundred has been achieved. There are two distinct advantages of employing the dilution system. First, the spectrometer can be operated with low net flow rates which result in shorter overall length and therefore smaller weight of the chamber. Second, accuracy in counting is increased because of low coincidence loss. The latter is important since the droplets are counted individually.

5. Method and calibration

a. Temperature fields on metal plates and in air space

Under the present arrangement for heating and cooling of our chamber, the temperature fields on the metal plates remain linear with distance in the direction perpendicular to the flow if heat does not escape out of the plates. In reality, heat transfer takes place in the vertical direction and, by deforming the field, it can unnecessarily complicate the problem. In order to alleviate this problem as discussed earlier, the rate of heat conduction through the plates was made seven times larger than that transferred between the plates (cf. Table 1). The latter heat transfer proceeds through three mechanisms, i.e., sensible heat transfer by air molecules, latent heat transfer accompanied by water vapor diffusion, and radiation heat transfer from the top to the bottom plates. In addition, the temperature profiles across the breadth of the chamber plates and the chamber height are monitored. Under this condition, a good linearity of the temperature profile across the breadth of the chamber plates was confirmed. The temperature profile across the chamber height was measured with an ultrafine thermocouple placed parallel to the isotherms and was found to be completely linear with height.

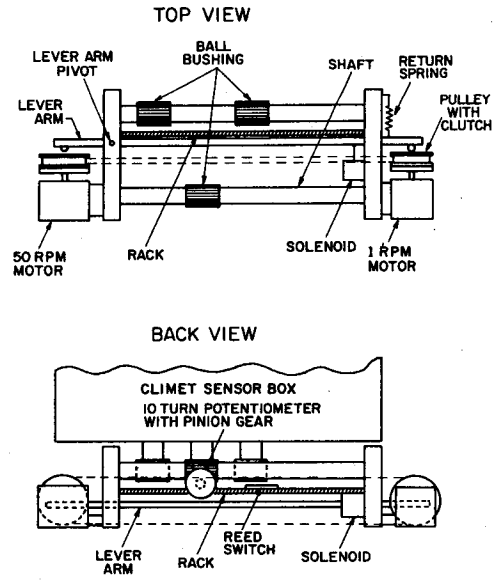

FIG. 6. An alternative scanning mechanism of the optical sensor, suitable for operations free of horizontal accelerations.

b. Supersaturation dependency of droplet growth time

The droplets begin to grow on the activated CCN as the sample air moves toward the end of the main chamber. The growth of these droplets is controlled by limiting the time period for moisture supply with respect to operating supersaturations. The profile of the filter paper glued with a spray contact cement underneath the top plate was fixed by a trial and error method being based on the calculations of Saxena and Carstens (1971) and a set of experiments carried out with variable sample-flow speed. These calculations are based on the assumptions that all CCN are hygroscopic NaCl nuclei and that droplet growth obeys the Maxwellian theory following an approach similar to that of Squires (1952).

For a given profile of the filter paper with the sampling tube at the end, the time available for droplet growth is inversely proportional to the flow rate. Therefore, by changing the flow rate with the sampling tube fixed at one position, one can examine the droplet growth process in the sample air along the flow direction. Such investigations were made at different supersaturations by determining the number concentration of droplets whose diameter exceeded 1.0, 1.5 and 2.0 μm; the results are shown in Fig. 7.

From Fig. 7, it is evident that for a supersaturation of 1.14%, the number concentration increases as the flow rate is reduced from 150 cm^3 s^{-1} since more time becomes available for droplet growth. A maximum value for the droplet concentration is thus achieved for a certain flow rate. If the flow rate is either faster or slower than this value, the concentration drops off. Comparison of curves for supersaturations of 0.28 and 1.18% shows that as the supersaturation increases, the optimum range of the flow rate, in which the concentration stays nearly constant, narrows down. This indicates that at larger supersaturations, the measured CCN concentration may strongly depend on the threshold droplet diameter. Another striking fact which may be seen in the figure is that, after the maximum number concentration being achieved under a given supersaturation, the number concentration steadily decreases toward lower flow rates instead of holding a constant value or a plateau before dropping suddenly. This tendency is stronger under high supersaturations.

At a given supersaturation, most of the droplets grow to a fixed detectable size within a definite time interval. However, as the droplets keep growing beyond the set detection limit, the differential gravitational settling or fallout of larger droplets reduces their number. This implies that nonuniformity in size must exist among formed droplets in order to account for the reduction of the number by differential settling. One of the possible reasons for the formation of such a wide droplet size distribution may be the variation of physico-chemical characteristics in CCN, and in this regard selection of a low supersaturation is equivalent to the narrowing down of the physico-chemical characteristics of the CCN such as activating more hygroscopic particles alone. For the same reason, selection of a larger detection size for formed droplets has an effect similar to lowering the supersaturation.

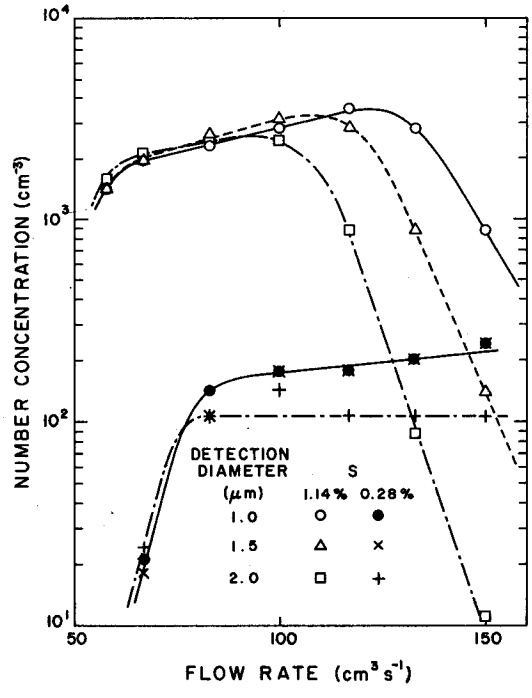

FIG. 7. Plot of the CCN number concentrations as a function of the sample flow rate for three different threshold droplet diameters. These measurements were made at two different positions in the spectrometer where the supersaturation was 0.28 and 1.14%, respectively. Therefore, the lengths of top-filter paper or droplet growth zones were different.

As we can see in Fig. 7, the number concentration for a relatively large detection size of droplets under a low supersaturation remains nearly constant due to the lack of differential settling loss, and yields a plateau as reported by Hudson and Squires (1973). Thus for a given sample, whether the plot for number concentration versus flow rate yields a plateau or not depends primarily on the detection size of droplets and the supersaturation.

As can be seen in Fig. 7, the maximum number concentration of activated CCN occurs at the right-hand shoulder of the sloped plateau. Since this value is the most logical choice for the number activated at the given supersaturation, it should be produced at the intake position of droplets for optical detection system in the spectrometer. The flow rate at which this maximum number concentration occurs can be used to determine the time interval required to grow the droplets to a given detection size. Such a time interval may be termed an optimum growth time, deviations from which on either side would result in reduction of the droplets. If we let t_m be the optimum growth time for a given supersaturation and v_m the corresponding linear velocity of the sample, then $d_f = t_m v_m$ would denote the necessary distance of the filter paper. Through the experimental determination of d_f for each supersaturation and iterating the procedure for the desired range of supersaturations, the profile of the top-plate filter paper can be determined.

It may be noted that the experimentally determined growth rate of droplets was much slower than that predicted by the Maxwellian theory. We believe this may be partly due to the fact that the values of the condensation or thermal accommodation coefficient or both are much smaller than unity (Fukuta and Walter, 1970). Droplet growth calculations based on the Maxwellian model are sufficient for the initial estimation of the profile of the top filter paper, for the trial and error adjustment to be performed later will include the accommodation coefficient effects. This approach is valid so long as the assumption holds that fixed average values of condensation and thermal accommodation coefficients exist and do not vary during the test.

Experimental values of the condensation coefficient, reported recently in the literature, vary from 1.0 to 0.03 (Chodes *et al.*, 1974; Sinnarwalla *et al.*, 1975) and they were determined under the common assumption that the thermal accommodation coefficient is unity. If the condensation coefficient is assumed to vary with the physico-chemical properties of the aerosol sample, it will influence the growth of droplets (Fukuta and Walter, 1970) and this, in turn, will not allow the setting of a single sample flow rate for measuring the entire CCN spectrum with our spectrometer or it would not allow the setting of a threshold droplet diameter for the entire range of the spectrum (Hoppel and Wojciechowski, 1976). Sketchy evidence exists that the value of the condensation coefficient depends on the amount of impurity present in the water droplet (for example, a condensation coefficient of 0.1 for pure water droplets and 0.02 for the droplet containing 10^{-17} moles of salt).

TABLE 2. Comparison of CCN counts obtained by automatic recording and direct photography of droplets.

Run no.	S (%)	Automatic recording (cm^{-3})	Direct photography (cm^{-3})	Deviation (%)
1	0.30	175	178	+1.7
2	0.40	259	219	−18.3
3	0.54	322	382	+15.7
4	0.69	512	410	−24.9
5	0.89	634	669	+5.2
6	1.1	741	806	+8.1
7	1.4	1060	1188	+10.8
8	1.8	1341	1325	−1.2
9	2.1	1483	1339	−10.7

The literature contains too few experimental measurements to hypothesize a correlation between the condensation and thermal accommodation coefficients and the physico-chemical nature of the aerosol. Our measurements in maritime, continental, polluted and unpolluted air masses do not indicate that a single sample flow-rate setting (typically, the volume flow rate is set in the range of 5–6 ℓ min^{-1}) is unable to monitor the entire CCN spectrum.

c. Evaporation of sample droplets

As the viewing volume in the sensor chamber is continuously being heated due to light beam and other power consuming devices surrounding it, it was decided to investigate the possible evaporation of the sample droplets. Since the particle detecting assembly counts the particles by sizing them according to a set threshold value, the recorded concentration becomes a function of the particle size. For our experiments, the threshold was set at 1 μm in diameter. All particles larger than this size were counted. Our experimental study revealed that if the sheath air temperature is higher than the median plane temperature, evaporation of the sample droplets occurs. For optimum operation of the spectrometer, the median plane temperature should be kept ~1–4°C higher than the sheath air temperature; alternatively, the sheath air should be thermostated and kept at the same temperature as that of the median plane.

d. Cross-check of the present counting technique with the photographic method

In order to check the present method of particle counting, a cross-check was made with the direct photographing method. For the test, an air sample was stored in a 1100 ℓ capacity Mylar bag and a collimated mercury-arc light beam, 6.1 mm in diameter,

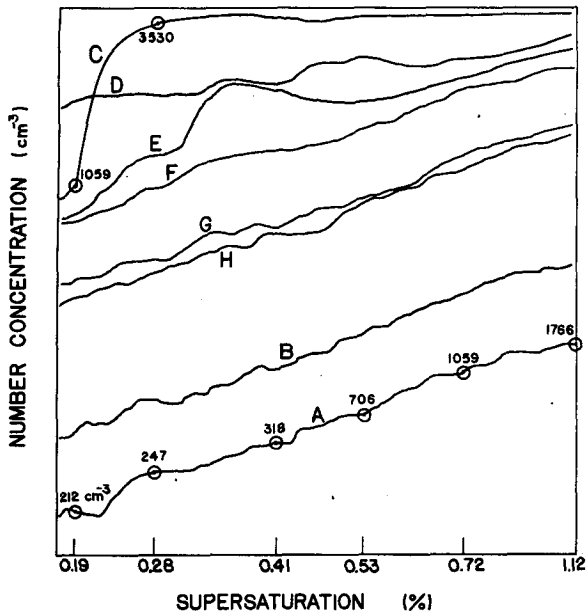

FIG. 8. Detection of a passing smoke plume by the CCN spectrometer. The scale is logarithmic along the ordinate and nonlinear along the abscissa. Plots A, B: background CCN spectra; plot C: plume peak in the spectrum; plots D–H: the spectra taken successively at 15 s intervals, thereafter. Plot H represents the background spectrum after the smoke peak passed. Zero points are shifted vertically at a given interval for plots A–C in the manner described in the text and then fixed for the rest of them.

was passed across the breadth of the chamber at the exit end. The photographs were taken at right angles to the light beam after stopping the sample flow momentarily. The results are summarized in Table 2. The counts obtained by the two methods agree with an absolute average deviation (treating the direct photographic counts as a standard concentration) of 10.7%. This supports the accuracy of the present photoelectronic counting method which avoids errors from manual handlings (such as the counting of droplets on photographic plates).

With the present setup, the range of the photoelectric counting method is from 4–35 000 particles cm^{-3}. With the dilution system of a factor of 100, the actual sample flow rate for counting is 1.2 cm^3 s^{-1}. In ~15 s, the scanning tube traverses a distance of ~15 cm along the median plane of the chamber. Within a traverse distance of 1 cm, it therefore draws a sample of 1.2 cm^3 for counting the formed droplets. If the CCN concentration in the sample is too low, for example, 4 cm^{-3}, the probable error (proportional to the square root of the concentration) is quite large, i.e., 4±2 or 50%. On the other hand, if the CCN concentration is too high, for example, 35 000 cm^{-3}, the probable error is only 0.5% but the error due to coincidence losses (because two particles or more entering the sensing volume simultaneously) goes up as high as 11.6%. The sensing volume of the optical system is 0.8 mm^3. In practice, these two extremes are not encountered frequently.

6. Measurements on aerosols

An example of the real-time detection of a smoke plume, generated in the laboratory, is shown in Fig. 8, which is the actual reproduction of the record produced by the spectrometer. On the ordinate, the CCN concentration is recorded on the logarithmic scale and on the abscissa, the supersaturation is recorded on a nonlinear scale. As explained earlier, the X-Y recorder is programmed to advance the chart by a fixed distance at the end of each spectrum record. Plots A and B were recorded in this manner and represent the room aerosol. Plot C represents the generated smoke plume that arrived as concentrations jumped by an order of magnitude. After recording plot C, the advance of the X-Y chart was stopped and plots D–H were recorded on the same base line. As is evident from the figure after the plume passed, the CCN concentrations began to recede to background levels and plot H is almost identical to plot B (notice the slope) which represents the room aerosol. From the figure, it is clear that even without reducing the data, a glance of the chart provides information regarding variations in the test sample.

On 9 August 1974, field measurements of diurnal variations in the CCN spectrum were made. The observation point was established ~18.5 m above the ground at the southern outskirts of Denver County.

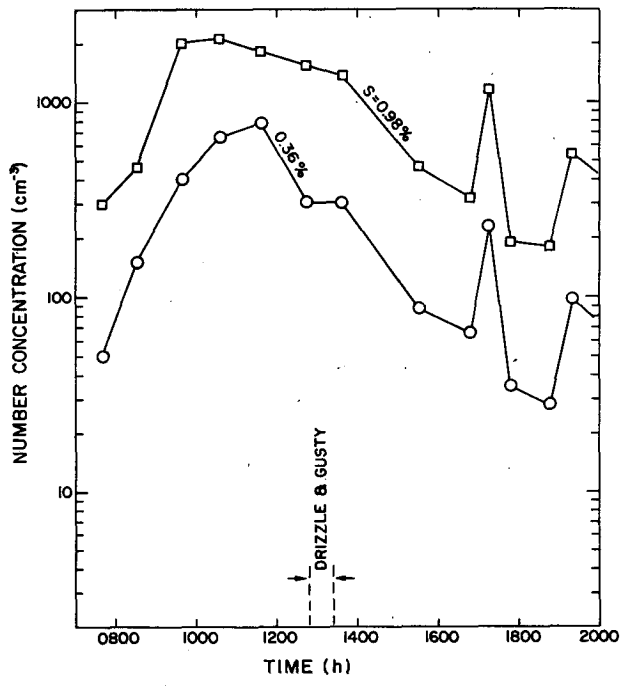

FIG. 9. CCN concentration obtained by the spectrometer on 9 August 1974 for the Denver aerosol (18.5 m above the ground).

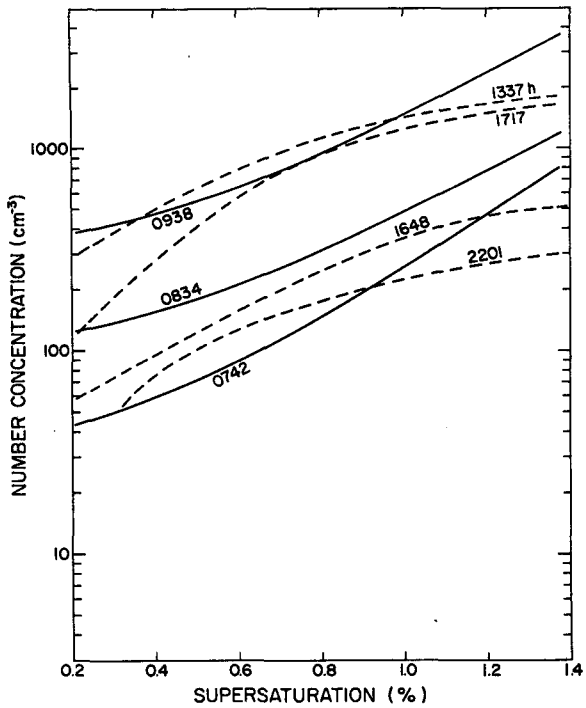

FIG. 10. CCN spectrum recorded at different times of the day on 9 August 1974 for the Denver aerosol (18.5 m above the ground).

Due care was taken to draw the natural atmospheric aerosol. The detected diurnal variations are shown in Figs. 9 and 10. In the early morning hours of 9 August, measurable precipitation was recorded at the sampling site followed by continuous drizzle for 3 h which stopped at 0730 LT. This indeed had a strong scavenging effect on CCN concentrations. A peak in the CCN concentration representative of an increase in the vehicular traffic during morning and evening hours is obvious (Fig. 9). Fig. 10 reveals that the CCN spectrum is concave upward with respect to the operating range of supersaturations during morning hours and convex upward during the afternoon and evening hours. One of the reasons for this interesting change may be the high concentration of the CCN active at low supersaturations during the later period as a result of the coagulation mechanism. The observed effect, however, is a combined result of the CCN generation and the coagulation processes. Sixteen CCN spectra were measured during the day. Each spectrum was fitted to the equation: $N=CS^k$, where C (cm^{-3}) and k and constant for the spectrum. The least-square-fit values of k showed that the slope of the spectrum varied from 0.6–1.8. The k values are similar to those reported by Braham (1974) for the St. Louis aerosol.

7. Concluding remarks

One of the roles played by the CCN is to interact with the supersaturation generated during the process of cloud formation and to influence the initial microphysical structure of clouds and fogs. For the interaction, the activation spectrum of the CCN is involved rather than the CCN at a specific level of supersaturation, and in order to understand the spectrum in terms of space and time, a device capable of rapidly and continuously determining the CCN spectrum is clearly needed. The new CCN spectrometer reported above was developed for this reason. Its major features are as follows:

1) A new horizontal thermal gradient diffusion chamber is employed to create a range of supersaturation.

2) Processing of the sample air is continuous.

3) The CCN are simultaneously activated under the range of supersaturation.

4) The sampling tube detects the activated CCN scanning through the range of supersaturation existing in different parts of the chamber and the output of the position-synchronized potentiometer indicates the supersaturation level. Simultaneous recording of the number concentration and the supersaturation on the X-Y plotter forms the concept of the CCN spectrum display.

5) A continuous recording X-Y plotter is used with a programmed chart shift and the CCN activity spectrum is displayed in real time.

6) A reversing mechanism of the scanner and an intermittent driving scheme of the recorder chart are successfully developed and employed.

7) A scheme of calibration for droplet growth time after activation is developed for the range of cloud supersaturations.

8) The CCN spectrometer is most suitable for airborne measurements. Its applications other than real-time CCN spectrum determination, such as plume tracking and identification, are possible due to its *in situ* and fast response features giving high space and time resolutions.

Acknowledgments. The authors are thankful to Messrs. Arpad Gorove and Franklin White for their help in fabricating the scanning mechanism. This work was supported by the National Science Foundation under Grants DES75-13361 and ATM 78-03588, and the Department of the Navy, Naval Air Systems Command, under Contract N00019-75-C-0310.

REFERENCES

Braham, Jr., R. R., 1974: Cloud physics of urban weather modification. A preliminary report. *Bull. Amer. Meteor. Soc.*, **55**, 100–106.

Chodes, N. J., J. Warner and A. Gagin, 1974: A determination of the condensation coefficient of water from the growth rate of small cloud droplets. *J. Atmos. Sci.*, **31**, 1351–1357.

Elliott, W. P., 1971: Dimensions of thermal diffusion chambers. *J. Atmos. Sci.*, **28**, 810–811.

Fitzgerald, J. W., 1970: Nonsteady-state supersaturations in the thermal diffusion chambers. *J. Atmos. Sci.*, **27**, 70–72.

Fukuta, N., and L. A. Walter, 1970: Kinetics of hydrometeor growth from a vapor-spherical model. *J. Atmos. Sci.*, **27**, 1160–1172.

——, and V. K. Saxena, 1977: A horizontal thermal gradient cloud condensation nucleus spectrometer: The theory of operation. *Proc. Ninth Int. Conf. Atmospheric Aerosols, Condensation and Ice Nuclei*, Galway, Ireland, Pergamon Press.

Gagin, A., and B. Terliuc, 1968: A modified Wieland-Twomey thermal diffusion cloud nuclei counter. *J. Rech. Atmos.*, **3**, 73–77.

Goroch, A., and J. Carstens, 1972: An analysis of wall effects in the modified Wieland-Twomey, thermal diffusion cloud nuclei counter of Gagin and Terliuc. *J. Rech. Atmos.*, **6**, 669–672.

Hoppel, W. A., and T. A. Wojciechowski, 1976: Accuracy limitations on CVN measurements with thermal gradient diffusion chambers. *J. Appl. Meteor.*, **15**, 107–112.

Hudson, J. G., and P. Squires, 1973: Evaluation of a recording continuous cloud nucleus counter. *J. Appl. Meteor.*, **12**, 175–183.

Jiusto, J. E., 1976: Cloud condensation nucleus counters. *Atmos. Tech.*, No. 8, 43–50.

Laktionov, A. G., 1967: On the connection between the condensation activity of irradiated nuclei and their sizes. *Izv. Atmos. Ocean. Phys.*, **3**, 25–33.

——, 1968: Photoelectric measurements of condensation cloud nuclei. *J. Rech. Atmos.*, **3**, 63–70.

Naruse, H., 1978: On an improvement of the thermal diffusion chamber for cloud nuclei measurement and some measurements around the paper mills. *Meteor. Geophys. (Japan)*, **29**, 141–150.

Radke, L. F., and J. E. Jiusto, 1977: Cloud condensation nuclei counter: A review. *Proc. Ninth Int. Conf. Atmospheric Aerosols, Condensation, and Ice Nuclei*, Galway, Ireland, Pergamon Press.

Saxana, V. K., and J. C. Carstens, 1971: On the operation of cylindrical thermal diffusion cloud chambers. *J. Rech. Atmos.*, **5**, 11–23.

——, and J. L. Fowler, 1973: Experimental investigation of transient supersaturations in a thermal diffusion chamber. *J. Appl. Meteor.*, **12**, 984–990.

——, J. N. Burford and J. L. Kassner, Jr., 1970: Operation of a thermal diffusion chamber for measurements on cloud condensation nuclei. *J. Atmos. Sci.*, **27**, 73–80.

Severynse, G. T., 1964: A portable cloud nuclei counter. *J. Rech. Atmos.*, **1**, 11–16.

Sinnarwalla, A. M., and D. J. Alofs, 1973: A cloud nucleus counter with long available growth time. *J. Appl. Meteor.*, **12**, 831–835.

——, —— and J. C. Carstens, 1975: Measurements of growth rate to determine condensation coefficients for water drops grown on natural cloud nuclei. *J. Atmos. Sci.*, **32**, 592–599.

Storozhilova, A. I., 1961: A differential counter for condensation nuclei. *Researches in the Field of Surface Forces*, Akad. Nauk SSR, Moscow, 209–211.

Squires, P., 1952: The growth of cloud drops by condensation. *Aust. J. Sci. Res.*, **A5**, 59–86.

Tomlinson, E. M., and N. Fukuta, 1979: Aspect ratio of thermal diffusion chambers. *J. Atmos. Sci.*, **36**, 1362–1365.

Twomey, S., 1963: Measurements of natural cloud nuclei. *J. Rech. Atmos.*, **1**, 101–105.